Research Article | Vol. 29, No. 24 / 22 Nov 2021 / Optics Express 39186
Optics EXPRESS

Broadband perfect transparency-to-absorption switching in tilted anisotropic metamaterials based on the anomalous Brewster effect

ZHIKAI MA,[1,4] HUIYING FAN,[1,2,4] HANG ZHOU,[1,5] MIN HUANG,[3,6] AND JIE LUO[1,2,7]

[1]School of Physical Science and Technology, Soochow University, Suzhou 215006, China
[2]Institute of Theoretical and Applied Physics, Soochow University, Suzhou, 215006, China
[3]School of Optoelectronic Science and Engineering & Collaborative Innovation Center of Suzhou Nano Science and Technology, Soochow University, Suzhou 215006, China
[4]These authors contributed equally to this work.
[5]hzhou@suda.edu.cn
[6]hmin@suda.edu.cn
[7]luojie@suda.edu.cn

Abstract: Dynamically switchable light transmission/absorption functionality is highly desirable in sensing and functional devices. However, the operating bandwidth of the newly emerging schemes using resonant meta-structures is inherently limited. In this work, we design and numerically demonstrate a non-resonant tilted anisotropic metamaterial consisting of phase-change materials. When the phase transition of the phase-change material from amorphous phase to crystalline phase occurs, the functionality of the metamaterial can be switched from perfect transparency to perfect absorption for transverse-magnetic polarization under oblique incidence over a broad spectrum. Such a remarkable phenomenon originates in the anomalous Brewster effect, which enables broadband reflectionless transmission/absorption of light under the anomalous Brewster's angle. Moreover, gradient metamaterials exhibiting dynamically controllable functionality for incident light with an almost arbitrary wavefront are demonstrated. The proposed metamaterials are simple but highly efficient, which may find applications in sensing and advanced and intelligent optical devices.

1. Introduction

The study of light manipulation has a long history and is of great importance in numerous electromagnetic and photonic applications. Recently, with the rise of metamaterials and metasurfaces that go beyond natural materials in many aspects, dynamic control of light becomes feasible by incorporating tunable materials [1–7], including liquid crystals [8–10], phase-change materials (PCMs) [11–17], etc. Up to now, various multifunctional meta-devices that can control light transmission, reflection, absorption and diffraction have been proposed [18–22]. The control of light transmission/absorption is shown in two extreme anomalies: perfect transmission or transparency [23,24] and perfect absorption [25–28]. Realizing dynamic switch between the two opposite anomalies is of particular interest. Very recently, the idea of the perfect transmission-to-absorption switching has been demonstrated in microwaves using metasurfaces incorporating PIN diodes [29–32]. In the infrared region, PCM-assisted metamaterials were proposed for polarization-insensitive functionality [33] and circular polarization [34]. However, due to the resonant nature of meta-structures, the operating bandwidth in these previous works is inherently limited. This would lead to restrictions on practical applications that require broad working bandwidth, such as broadband optical modulator [35] and thermal emission control [36,37].

#443790 https://doi.org/10.1364/OE.443790
Journal © 2021 Received 20 Sep 2021; revised 1 Nov 2021; accepted 1 Nov 2021; published 9 Nov 2021

Optics EXPRESS

In this work, we propose a non-resonant tilted anisotropic metamaterial (TAM) exhibiting broadband perfect transmission-to-absorption switching functionality in the infrared region. The dynamically switchable functionality is bestowed by its PCM component, which can switch between different phase states as a function of an external bias like heat [38,39], photon [40,41], or electric energy [42], offering a pronounced change of its dielectric function. We find that when the phase transition of PCM germanium telluride (GeTe) from amorphous phase to crystalline phase occurs, the functionality of the TAM can be switched from perfect transparency to perfect absorption over a broad spectrum. This rare effect is bestowed by the occurrence of anomalous Brewster effect, which establishes ultrabroadband impedance matching between free space and anisotropic absorptive materials, thus enabling reflectionless manipulation of light in an unprecedented wide spectrum [43,44]. Based on this principle, gradient TAMs exhibiting broadband perfect transmission-to-absorption switching functionality for incident light with almost arbitrary wavefront are further demonstrated. Compared with the previously reported schemes on transparency-to-absorption switching [29–34], our proposed TAMs are simple but of a clear advantage of broad operating bandwidth. Compared with the seminal works on anomalous Brewster effect [43,44], this work demonstrates a highly efficient approach to realize dynamic switching between two opposite anomalies, i.e. perfect transparency and perfect absorption, based on the anomalous Brewster effect, which may find applications in sensing, advanced and intelligent optical devices.

2. Dynamically controllable TAM and anomalous Brewster effect for reflectionless manipulation of light

The schematic graph of the proposed dynamically controllable TAM is shown in Fig. 1(a). It is composed of a periodic array of tilted ultrathin PCM GeTe films (relative permittivity $\varepsilon_{\mathrm{GeTe}}$, tilt angle α, thickness t along the normal direction of GeTe films) aligned along the y direction embedded in a dielectric host (relative permittivity ε_{d}, thickness d). The separation distance between two adjacent GeTe films is a along the y direction, which is much larger than t (i.e. $a \gg t$), but much smaller than free-space wavelength λ_0 (i.e. $a \ll \lambda_0$).

The GeTe is an especially promising PCM as it possesses the ability of rapidly switching between different phases in a reversible way. The phase transition can be achieved optically or through Joule heating and is proven to be reliable, fast, and repeatable. For instance, by using laser irradiation, the change in optical properties on the phase transition can be realized on the nanosecond timescale (<100 ns) [45]. We note that both crystalline and amorphous phases of GeTe are stable at room temperature, resulting in zero static power consumption [4,46]. Figures 1(c) and 1(d) show, respectively, the real and imaginary parts of its relative permittivity $\varepsilon_{\mathrm{GeTe}}$ in amorphous (blue lines) and crystalline (red lines) phases, which are taken from [4]. We see that the loss coefficient of GeTe is negligibly small in amorphous phase over the spectrum of 3-11μm, as the amorphous GeTe possesses a "window of low losses" in the mid-infrared frequency range [4,47]. While the loss coefficient is quite large in crystalline state. This unique property provides us a route to dynamically switch the functionality of the TAM from perfect transparency (upper panel) to perfect absorption (lower panel) over a broad spectrum, as illustrated in Fig. 1(a).

Here, we study the TAM from the perspective of effective medium model. Since the TAM satisfies $a \ll \lambda_0$, it can be approximately homogenized as an effective anisotropic medium with $\varepsilon_{\perp} = \frac{a\varepsilon_{\mathrm{GeTe}}\varepsilon_{\mathrm{d}}\cos\alpha}{(a\cos\alpha - t)\varepsilon_{\mathrm{GeTe}} + t\varepsilon_{\mathrm{d}}}$ and $\varepsilon_{\parallel} = \varepsilon_{\mathrm{d}} + \frac{\varepsilon_{\mathrm{GeTe}} - \varepsilon_{\mathrm{d}}}{a\cos\alpha} t$ [48,49], which are, respectively, the effective permittivities normal and parallel to the GeTe films, as illustrated in Fig. 1(b). Considering the limit of $a \gg t$, the $\varepsilon_{\perp}$ can be simplified to $\varepsilon_{\perp} \approx \varepsilon_{\mathrm{d}}$.

Now, we assume a transverse-magnetic (TM, magnetic field along the x direction) polarized wave incident from dielectric background (relative permittivity ε_{b}) onto the TAM. The magnetic

Optics EXPRESS

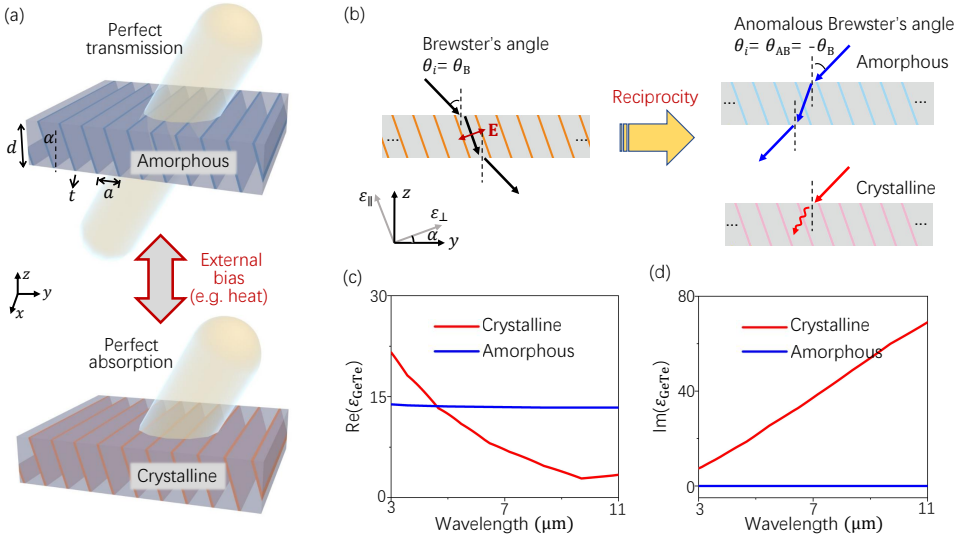

Fig. 1. (a) Schematic drawing of a dynamically controllable TAM consisting of a sub-wavelength tilted PCM film array embedded in a dielectric host, whose functionality can be switched from perfect transparency (upper) to perfect absorption (lower) under external bias. (b) Left panel: perfect transparency due to the traditional Brewster effect under $\theta_i = \theta_B$. Right panel: perfect transparency in amorphous phase (upper) and perfect absorption in crystalline phase (lower) due to the anomalous Brewster effect under $\theta_i = \theta_{AB} = -\theta_B$. (c) Real and (d) imaginary parts of the relative permittivity ε_{GeTe} of PCM GeTe in amorphous (blue lines) and crystalline (red lines) phases.

fields of the incident and reflected waves can be expressed as

$$\mathbf{H}_{in} = \hat{x} H_0 e^{i(k_y y + k_{b,z} z) - i\omega t}, \tag{1}$$

$$\mathbf{H}_{re} = \hat{x} r H_0 e^{i(k_y y - k_{b,z} z) - i\omega t}, \tag{2}$$

where H_0 is the magnetic-field amplitude, and r is the reflection coefficient. The k_y and $k_{b,z}$ are, respectively, the y- and z-components of wave vector in the background. For an incident angle of θ_i, we have $k_y = \sqrt{\varepsilon_b} k_0 \sin\theta_i$ with k_0 $(= 2\pi/\lambda_0)$ being the wave number in free space. The relation between the $k_{b,z}$ and k_z is described by the dispersion relation:

$$k_y^2 + k_{b,z}^2 = \varepsilon_b k_0^2. \tag{3}$$

The magnetic field of transmitted wave in the TAM can be expressed as

$$\mathbf{H}_{tr} = \hat{x} t H_0 e^{i(k_y y + k_z z) - i\omega t}, \tag{4}$$

where t is the transmission coefficient. Substituting Eq. (4) into the wave equation $\nabla \times \left[\varepsilon^{--1}(\nabla \times \mathbf{H})\right] = k_0^2 \mathbf{H}$ yields the dispersion relation:

$$k_y^2 \varepsilon_{yy} + k_z^2 \varepsilon_{zz} + k_y k_z (\varepsilon_{yz} + \varepsilon_{zy}) = (\varepsilon_{yy}\varepsilon_{zz} - \varepsilon_{yz}\varepsilon_{zy}) k_0^2, \tag{5}$$

Optics EXPRESS

where ε_{ij} ($i,j = y$ or z) denotes the component of the relative permittivity tensor $\bar{\varepsilon}$ in the global Cartesian coordinate system (x, y, z):

$$\bar{\varepsilon} = \begin{pmatrix} \varepsilon_{xx} & 0 & 0 \\ 0 & \varepsilon_{yy} & \varepsilon_{yz} \\ 0 & \varepsilon_{zy} & \varepsilon_{zz} \end{pmatrix} = \begin{pmatrix} \varepsilon_{\parallel} & 0 & 0 \\ 0 & \varepsilon_{\perp}\cos^2\alpha + \varepsilon_{\parallel}\sin^2\alpha & (\varepsilon_{\perp} - \varepsilon_{\parallel})\sin\alpha\cos\alpha \\ 0 & (\varepsilon_{\perp} - \varepsilon_{\parallel})\sin\alpha\cos\alpha & \varepsilon_{\perp}\sin^2\alpha + \varepsilon_{\parallel}\cos^2\alpha \end{pmatrix}. \quad (6)$$

Considering the continuity boundary conditions of tangential electric and magnetic fields at the air-TAM interface, the reflection coefficient r can be derived as,

$$r = \frac{(\varepsilon_{yy}\varepsilon_{zz} - \varepsilon_{yz}\varepsilon_{zy})k_{b,z} - \varepsilon_b(\varepsilon_{yz}k_y + \varepsilon_{zz}k_z)}{(\varepsilon_{yy}\varepsilon_{zz} - \varepsilon_{yz}\varepsilon_{zy})k_{b,z} + \varepsilon_b(\varepsilon_{yz}k_y + \varepsilon_{zz}k_z)}. \quad (7)$$

By substituting the permittivity tensor (Eq. (6)) and dispersion relations (Eqs. (3) and (5)) into Eq. (7), the zero-reflection condition (i.e., $r = 0$) can be derived as,

$$\varepsilon_{\perp}\varepsilon_{\parallel}k_0^2\cos^2\theta_i + \varepsilon_b k_0^2[\varepsilon_b\sin^2\theta_i - (\varepsilon_{\perp}\sin^2\alpha + \varepsilon_{\parallel}\cos^2\alpha)] = 0. \quad (8)$$

Here, we are more interested in a unique solution of Eq. (8) that is $\varepsilon_{\parallel}$-independent. This requires that the first derivative of the left term in Eq. (8) versus $\varepsilon_{\parallel}$ is zero, thus we have $\varepsilon_d\cos^2\theta_i = \varepsilon_b\cos^2\alpha$. Substituting this condition into Eq. (8) yields,

$$(\varepsilon_b - \varepsilon_d\tan^2\alpha)(\varepsilon_b - \varepsilon_d) = 0. \quad (9)$$

Equation (9) is the condition of $\varepsilon_{\parallel}$-independent zero reflection. We note that the $\varepsilon_{\parallel}$-independence is equivalent to the $\varepsilon_{\mathrm{GeTe}}$-independence as $\varepsilon_{\perp}$ is irrespective of $\varepsilon_{\mathrm{GeTe}}$. Therefore, when the condition of Eq. (9) is fulfilled, we will always have zero reflection, irrespective of the phase states of GeTe. This endows the TAM with a remarkable ability of reflectionless manipulation of light through switching the phase states of GeTe.

When $\varepsilon_b \neq \varepsilon_d$, the solution of Eq. (9) is

$$\theta_i = \pm(\pi/2 - \alpha) \quad \text{with} \quad \alpha = \arctan\sqrt{\varepsilon_b/\varepsilon_d}. \quad (10)$$

One may notice that the required incident angle by Eq. (10) is the Brewster's angle θ_B [50] at the interface of background dielectric and TAM in the absence of GeTe films. Figure 1(b) presents a geometrical interpretation of this result. First, we assume a TAM without GeTe films. Reflection disappears under the Brewster's angle $\theta_B = \arctan\sqrt{\varepsilon_d/\varepsilon_b}$, and the refracted light is normal to the direction of specular reflection [50]. Thus, the angle of refraction is found to be $\pi/2 - \theta_B$. Then, we insert ultrathin GeTe films parallel to the direction of refracted light (i.e. $\alpha = \pi/2 - \theta_B$) in the dielectric host, such that the electric field $\mathbf{E}$ of refracted light is perpendicular to the GeTe films. Interestingly, in this case, the Brewster effect won't be destroyed as the refracted light cannot "see" such ultrathin GeTe films [51], and therefore the zero reflection preserves irrespective of the presence of GeTe films, as illustrated in the left panel of Fig. 1(b).

It becomes interesting when the reciprocity principle [52] is applied when flipping the incident angle from θ_B to $-\theta_B$ (right panel of Fig. 1(b)). According to the reciprocity principle, the reflection coefficients are exactly the same under incident angles of $\pm\theta_i$ for reciprocal media, i.e., $r(\theta_i) = r(-\theta_i)$ [52]. Therefore, the zero reflection remains unchanged irrespective of the existence of GeTe films. However, different from the situation under the incident angle of θ_B, the refracted light under $-\theta_B$ is no longer normal to the direction of specular reflection, and would be affected by the GeTe films as its electric field is no longer perpendicular to the GeTe films. In this sense, we denote the angle $-\theta_B$ as anomalous Brewster's angle $\theta_{AB} \equiv -\theta_B$, and

Optics EXPRESS

the reflectionless phenomenon as anomalous Brewster effect [43,44], which endows the TAM with an extraordinary ability of reflectionless manipulation of light, including tunable refraction and absorption. Through switching the GeTe from amorphous phase to crystalline phase, the functionality of the TAM can be switched from perfect transparency to perfect absorption for TM-polarized light under $\theta_i = \theta_{\mathrm{AB}}$.

It is noteworthy that the operating bandwidth in principle can cover an ultra-broad spectrum, far beyond those techniques based on resonant meta-structures [29–34]. From Eq. (10), we see that the anomalous Brewster's angle and the zero-reflection behavior are solely determined by the permittivities ε_{b} and ε_{d}. When utilizing dielectric materials possessing low dissipation loss and low chromatic dispersion, such as silica (SiO_2) and silicon (Si) in the infrared region, perfect transmission-to-absorption switching can be realized over a broad spectrum.

3. Numerical proof of broadband perfect transmission-to-absorption switching

Figure 2 shows direct numerical proof of the above theory. Here we choose air as the background ($\varepsilon_{\mathrm{b}} = 1$), and SiO_2 as the host of TAM. The geometrical parameters of the TAM are set as $d = 5\mu$m, $a = 500$nm and $t = 50$nm. Dispersive permittivity of SiO_2 is considered in the calculation of reflection, transmission and absorption in the following, which is taken from [53]. We shall note that the tilt angle of GeTe films would vary with working wavelength according to Eq. (10). However, we notice that the chromatic dispersion of SiO_2 is relatively low in the wavelength range of 3-7μm. Therefore, we approximately choose the averaged relative permittivity (~1.796) in this wavelength range to obtain a fixed tilt angle, i.e. $\alpha = 36.73°$. Then, the traditional (or anomalous) Brewster's angle is $\theta_{\mathrm{B}} = 53.27°$ (or $\theta_{\mathrm{AB}} = -53.27°$).

We first consider the TAM with GeTe in amorphous phase. Figure 2(a) shows simulated normalized magnetic-field H_x/H_0 distributions under the illumination of TM-polarized light of $\lambda_0 = 7\mu$m with $\theta_i = \theta_{\mathrm{B}}$ (left) and $\theta_i = \theta_{\mathrm{AB}}$ (right). H_x is the x-component of magnetic field. The simulation is performed using the software COMSOL Multiphysics. Periodic boundary conditions are set on the left and right boundaries. A port is set on the upper boundary to generate TM-polarized plane waves under oblique incidence of θ_i, and another port is set on the lower boundary to evaluate and absorb the transmitted waves. In Fig. 2(a), perfectly reflectionless transmission is observed. We note that when considering an imaginary part of $\varepsilon_{\mathrm{GeTe}}$ of 0.05, the transmittance is still as high as 0.99. For further verification, the reflectance R, transmittance T and absorptance A as the function of the incident angle θ_i are plotted in Fig. 2(b). The solid lines and dots denote, respectively, the theoretical results of the effective medium model using transfer matrix method [54] and numerical results of the actual TAM using the software COMSOL Multiphysics, showing very good coincidence. From Fig. 2(b), we clearly see total transmission under $\theta_i = \theta_{\mathrm{B}}$ and $\theta_i = \theta_{\mathrm{AB}}$. Moreover, we calculate the R and T of the actual TAM with respect to the working wavelength λ_0, as plotted in Figs. 2(b) and 2(c), respectively. Zero reflection and complete transmission under θ_{B} and θ_{AB} are observed over the spectrum of 3-7μm, demonstrating the broadband perfect transparency of the TAM with GeTe in amorphous phase for incident light under θ_{B} and θ_{AB}.

Then, we consider the crystalline phase of GeTe, in which case the GeTe is a lossy material. The simulated H_x/H_0-distribution in Fig. 3(a) shows an extreme angular asymmetric behavior, that is, perfect transmission under $\theta_i = \theta_{\mathrm{B}}$ (left), while perfect absorption under $\theta_i = \theta_{\mathrm{AB}}$ due to the anomalous Brewster effect (right) [44]. We note that in the case of $\theta_i = \theta_{\mathrm{B}}$, the refracted light in the TAM cannot "see" the GeTe films, thus maintaining the perfect transmission. Intriguingly, in the case of $\theta_i = \theta_{\mathrm{AB}}$, the electric field of the refracted light is no long perpendicular to the GeTe films. In this case, the incident energy would be dissipated on lossy GeTe films. Meanwhile, zero reflection remains as strictly protected by the reciprocity principle. This is because the reflection coefficients are exactly the same under incident angles of $\pm\theta_i$ for reciprocal media, i.e., $r(\theta_i) = r(-\theta_i)$ [52]. Such an extreme angular asymmetric behavior is further demonstrated by

Optics EXPRESS

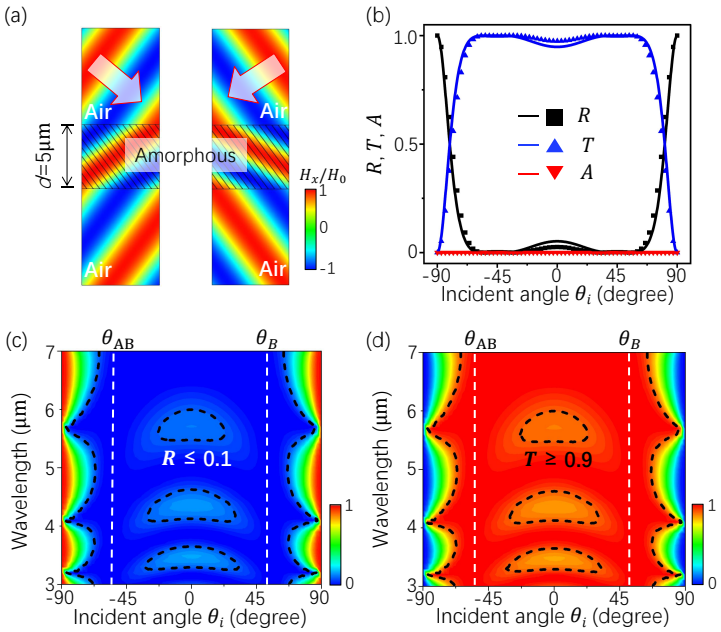

Fig. 2. (a) Simulated H_x/H_0-distributions in the TAM with GeTe in amorphous phase when TM-polarized light of $\lambda_0 = 7\mu$m is incident from air under $\theta_i = \theta_B = 53.27°$ (left) and $\theta_i = \theta_{AB} = -53.27°$ (right). The TAM consists of tilted GeTe films ($a = 500$nm, $t = 50$nm, $\alpha = 36.73°$) in a SiO_2 host with a thickness of $d = 5\mu$m. (b) Reflectance R, transmittance T and absorptance A as the function of incident angle at $\lambda_0 = 7\mu$m. The solid lines and dots denote, respectively, the theoretical results of the effective medium model and numerical results of the actual TAM. (c) Reflectance R and (d) transmittance T of the actual TAM as functions of the incident angle and working wavelength. The areas bounded by the black dashed lines denote the regions with $R \le 0.1$ in (c) and $T \ge 0.9$ in (d). The white dashed lines denote the Brewster's angle $\theta_B = 53.27°$ and anomalous Brewster's angle $\theta_{AB} = -53.27°$.

both theoretical results of the effective medium model (solid lines) and numerical results of the actual TAM (dots), as presented in in Fig. 3(b). Moreover, we find that the reflectionless high absorption under $\theta_i = \theta_{AB}$ can be obtained over a broad spectrum, as shown by the reflectance R and absorptance A in Figs. 3(c) and 3(d), respectively. Notably, the absorptance under $\theta_i = \theta_{AB}$ can be further increased to be unity for all wavelengths through simply increasing the thickness d of the TAM, thus realizing broadband perfect absorption in crystalline state.

The above results manifest that the functionality of the TAM can be tuned from perfect transparency to perfect absorption over a broad spectrum through changing the phase states under the anomalous Brewster's angle θ_{AB}. Although the spectrum of 3-7μm is considered here, the operating bandwidth actually can be further broadened as long as the dissipation loss and chromatic dispersion of the dielectric host are small and the effective medium approximation of the TAM is valid.

We note that the TAM is quite flexible in the material selection of the dielectric host. For demonstration, we compare the performance of TAMs with dielectric hosts made of SiO_2 and Si, whose relative permittivities are marked by vertical dashed lines in Fig. 4(a). Based on Eq. (10), the required tilt angle α and the corresponding θ_{AB} are plotted in Fig. 4(a). Figures 4(b) and 4(c) show, respectively, transmission spectrum in amorphous phase and absorption spectrum

Optics EXPRESS

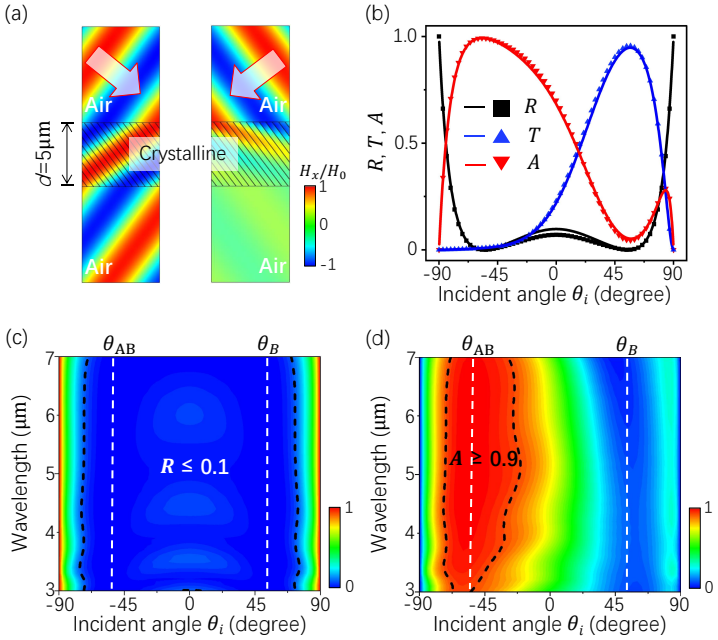

Fig. 3. (a) Simulated H_x/H_0-distributions in the TAM with GeTe in crystalline phase when TM-polarized light of $\lambda_0 = 7\mu$m is incident from air under $\theta_i = \theta_B = 53.27°$ (left) and $\theta_i = \theta_{AB} = -53.27°$ (right). The TAM consists of tilted GeTe films ($a = 500$nm, $t = 50$nm, $\alpha = 36.73°$) in a SiO_2 host with a thickness of $d = 5\mu$m. (b) Reflectance R, transmittance T and absorptance A as the function of incident angle at $\lambda_0 = 7\mu$m. The solid lines and dots denote, respectively, the theoretical results of the effective medium model and numerical results of the actual TAM. (c) Reflectance R and (d) absorptance A of the actual TAM as functions of the incident angle and working wavelength. The areas bounded by the black dashed lines denote the regions with $R \leq 0.1$ in (c) and $A \geq 0.9$ in (d). The white dashed lines denote the Brewster's angle $\theta_B = 53.27°$ and anomalous Brewster's angle $\theta_{AB} = -53.27°$.

in crystalline phase when $\theta_i = \theta_{AB}$. The TAM is the same as that in Figs. 2 and 3 except that different kinds of dielectric hosts are utilized here. Since the θ_{AB} relies on ε_d, the incident angle θ_i is changed accordingly for different dielectric hosts. It is seen that near-perfect transmission in amorphous phase and high absorption in crystalline phase are obtained over the spectrum of 3-7μm.

It is noteworthy that the imperfection of absorption in Fig. 4(c) attributes to finite decay rate and limited thickness d of the TAM. To quantitively evaluate the decay rate of the wave in the TAM, we rewrite the magnetic field in TAM (i.e. Equation (4)) as

$$\mathbf{H}_{tr} = \hat{x}tH_0 e^{-\kappa z} e^{i(k_y y + k_z' z) - i\omega t} \tag{11}$$

where k_z' and κ are, respectively, the real and imaginary parts of k_z. In the presence of material loss, the wave in the TAM decays exponentially at a rate $|\kappa|$. Since there is no reflection under the anomalous Brewster's angle, a larger decay rate indicates the higher absorption efficiency.

Base on the dispersion relation of Eq. (5), we plot the normalized decay rate $|\kappa|/k_0$ with respect to ε_d (black solid lines in Fig. 4(d)). The vertical dashed lines denote the values of ε_d of SiO_2 and Si. We find that the decay rate decreases when the dielectric host is changed from SiO_2 to Si, thus leading to relatively low absorption in the TAM with a Si host, as observed in Fig. 4(c). For visualization, we simulate the H_x/H_0-distributions in the TAM with a SiO_2 (left) or Si (right)

Optics EXPRESS

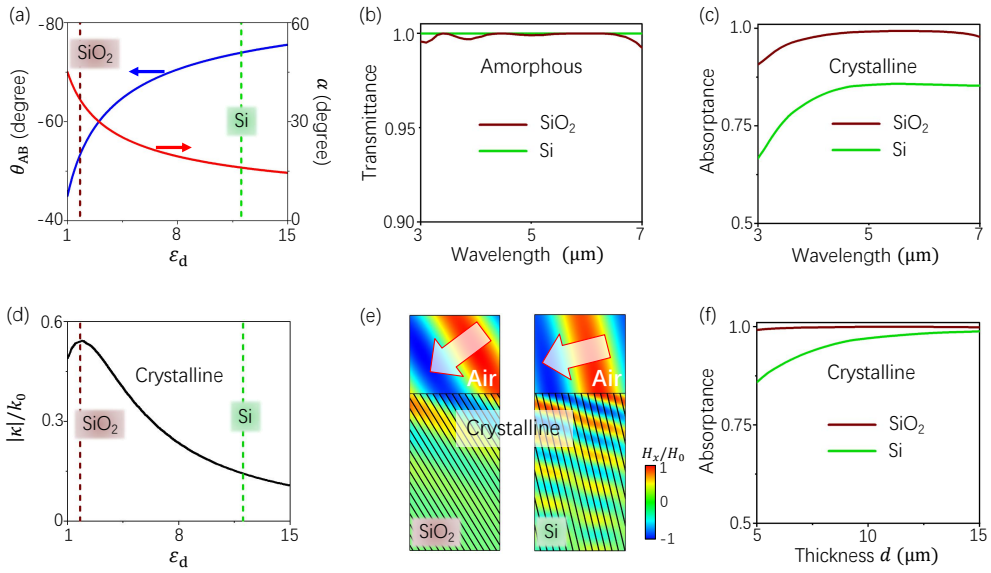

Fig. 4. (a) The anomalous Brewster's angle θ_{AB} and tilt angle α as a function of the relative permittivity ε_d of dielectric host based on Eq. (10). The vertical dashed lines denote the values of ε_d of SiO_2 and Si. (b) Transmission spectrum in amorphous phase and (c) absorption spectrum in crystalline phase. The TAM is the same as that in Figs. 2 and 3 except for the material of dielectric host. (d) Normalized decay rate of waves in TAM with GeTe in crystalline phase as the function of ε_d (black solid lines). The vertical dashed lines denote the values of ε_d of SiO_2 and Si. (e) Simulated H_x/H_0-distributions when the host dielectric material is SiO_2 (left) or Si (right). (f) Absorptance by the TAM with GeTe in crystalline phase with increasing the thickness d. In (b)-(f), the wavelength of incidence is 7μm, and the incident angle is the anomalous Brewster's angle.

host under the anomalous Brewster angle θ_{AB}, as shown in Fig. 4(e). We see that the wave in the TAM with a SiO_2 host decays more quickly than that in the TAM with a Si host. We note that the reflection is absent under the anomalous Brewster angle, therefore we can easily increase the light absorption to near-100% through simply increasing the thickness d of the TAM, as verified in Fig. 4(f). These results demonstrate the flexibility in the material selection of the dielectric host. As long as the TAM is thick enough, the broadband perfect transmission-to-absorption switching is realizable.

It is noteworthy that the broadband switching functionality is robust against the variations of geometrical parameters. In Fig. 5(a), the separation distance a between two adjacent GeTe films is changed from 500 nm to 1000 nm when the thickness of GeTe films is fixed at t = 50nm and $\alpha = 36.73°$. The blue and red lines denote, respectively, transmittance through the TAM with GeTe in amorphous phase and absorptance by the TAM with GeTe in crystalline phase under the anomalous Brewster's angle $\theta_{AB} = -53.27°$ at λ_0 = 7μm. The TAM is the same as that in Figs. 2 and 3 except that the a is changed. We see that the near-perfect transmission in amorphous phase is almost unchanged, and the absorption in crystalline phase is still very high (>0.98), showing a robust near-perfect switching behavior. Moreover, in Fig. 5(b), the thickness t of GeTe films is changed from 40 nm to 100 nm with fixed a = 500nm and $\alpha = 36.73°$. In Fig. 5(c), the tilt angle α is changed from 33.06° to 40.40° with fixed a = 500nm and t = 50nm. Still, the switching between near-perfect transmission in amorphous phase (blue lines) and high absorption in crystalline phase (red lines) is observed.

Optics EXPRESS

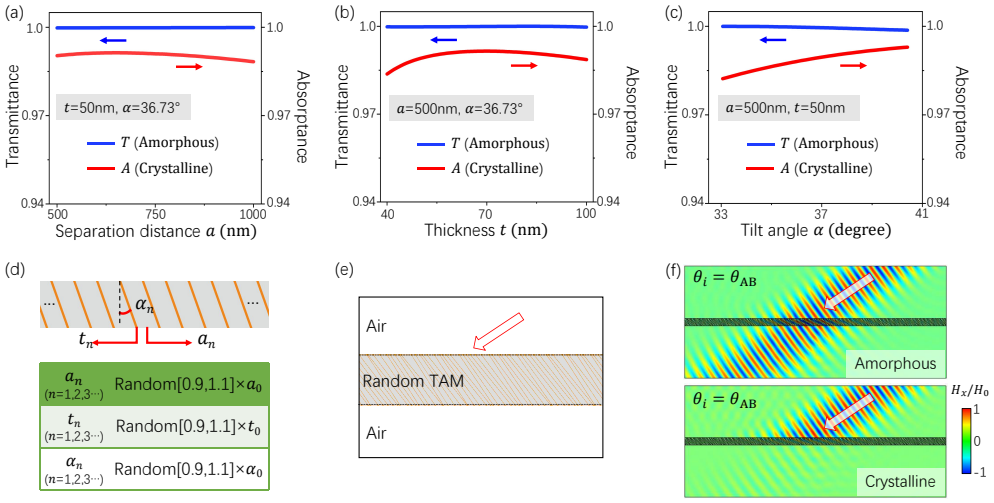

Fig. 5. [(a)-(c)] Transmittance through the TAM with GeTe in amorphous phase (blue lines) and absorptance by the TAM with GeTe in crystalline phase (red lines) when (a) the separation distance a is changed with fixed t = 50nm and α = 36.73°, (b) the thickness of GeTe films t is changed with fixed a = 500nm and α = 36.73°, (c) the tilt angle α is changed with fixed a = 500nm and t = 50nm. The TAM is the same as that in Figs. 2 and 3 except that the a, t or α is changed. The wavelength is 7μm, and the incident angle is $\theta_{AB} = -53.27°$, i.e. the anomalous Brewster's angle. (d) Schematic graph of a TAM with random a, t and α in different transversal positions. The a varies randomly in the range from $0.9a_0$ to $1.1a_0$ with a_0 = 500nm, the t varies randomly in the range from $0.9t_0$ to $1.1t_0$ with t_0 = 50nm, and the α varies randomly in the range from $0.9\alpha_0$ to $1.1\alpha_0$ with α_0 = 36.73°. (e) Illustration of the random TAM slab in the air background. (f) Simulated H_x/H_0-distributions under the illumination of a TM-polarized Gaussian beam under $\theta_{AB} = -53.27°$ at λ_0 = 7μm when the GeTe is in amorphous (upper) or crystalline (lower) phase.

For further verification of the robustness against the variations of geometrical parameters. We consider a TAM with random a, t and α in different transversal positions, as shown schematically in Fig. 5(d). The a varies randomly in the range from $0.9a_0$ to $1.1a_0$ with a_0 = 500nm, the t varies randomly in the range from $0.9t_0$ to $1.1t_0$ with t_0 = 50nm, and the α varies randomly in the range from $0.9\alpha_0$ to $1.1\alpha_0$ with α_0 = 36.73°. Figure 5(e) illustrates the random TAM slab in the air background. Figure 5(f) presents the H_x/H_0-distribution under the illumination of a TM-polarized Gaussian beam under the anomalous Brewster's angle $\theta_{AB} = -53.27°$ at λ_0 = 7μm. In the simulation, transition boundary condition is applied to the GeTe films for simplicity. The upper (or lower) panel denotes the TAM with GeTe in amorphous (or crystalline) phase. The simulation results clearly show the occurrence of near-perfect transmission in amorphous phase and near-perfect absorption in crystalline phase. These results demonstrate the robustness of near-perfect transmission-to-absorption switching functionality in the presence of imperfections, which cloud facilitate practical fabrication in experiments.

4. Gradient TAMs exhibiting broadband perfect transmission-to-absorption switching for light with an almost arbitrary wavefront

In the above, we have demonstrated the broadband perfect transmission-to-absorption switching in the case of $\varepsilon_b \neq \varepsilon_d$ (i.e., the host dielectric material of TAM is different from the background dielectric material), which requires a particular tilt angle α (Eq. (10)) when the host of TAM is

Optics EXPRESS

fixed. In the following, we'd like to show the solution of Eq. (10) in the case of $\varepsilon_b = \varepsilon_d$, that is, the host dielectric material of TAM is the same as the background dielectric material. In this case, the value of α can be arbitrarily chosen irrespective of the material selection of the dielectric host of TAM, that is,

$$\theta_i = \pm\alpha \quad \text{with} \quad \alpha \quad \text{being arbitrary.} \tag{12}$$

As an example, we assume that both the background and host dielectric materials are SiO_2, as illustrated in Fig. 6(a). Based on effective medium model and Eq. (7), the reflectance at SiO_2-TAM interface with respect to α and θ_i for TM-polarized light of $\lambda_0 = 7\mu m$ is calculated, as presented in Fig. 6(b). The geometrical parameters of the TAM are $a = 500nm$ and $t = 50nm$. As expected, zero reflection can be obtained for any value of α as long as the condition $\theta_i = \pm\alpha$ is satisfied. For further verification, in Fig. 6(c) we simulate the H_x/H_0-distributions when TM-polarized light is incident from SiO_2 onto the TAM ($\alpha = 45°$, $d = 5\mu m$) with GeTe in amorphous (left) or crystalline (right) phase under the incident angle of $\theta_i = -45°$. Clearly, the switching between perfect transmission and perfect absorption is observed when the phase transition of GeTe occurs. Moreover, in Fig. 6(d) we change the rotation angle α to 60° and re-simulate the H_x/H_0-distributions under $\theta_i = -60°$, also showing the perfect switching functionality. These results demonstrate that the perfect transmission-to-absorption switching behavior can be obtained for any value of α as long as the condition $\theta_i = \pm\alpha$ is satisfied. We shall note that the operating bandwidth can also cover a broad regime due to the non-resonant nature of the proposed TAM.

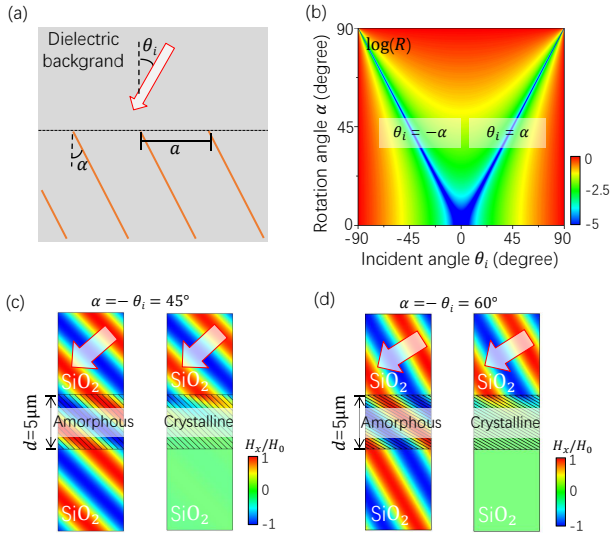

Fig. 6. (a) Illustration of a TAM in a dielectric background. The host dielectric material of the TAM is the same as the background dielectric material. (b) Reflectance at the SiO_2-TAM interface as functions of the incident angle θ_i and tilt angle α for TM-polarized light of $\lambda_0 = 7\mu m$. The TAM consists of periodic tilted GeTe films with $a = 500nm$ and $t = 50nm$ in a SiO_2 host. The calculation is based on the effective medium model and Eq. (7). [(c) and (d)] Simulated H_x/H_0-distributions for TM-polarized light of $\lambda_0 = 7\mu m$ incident from SiO_2 under (c) $\theta_i = -45°$ and (d) $\theta_i = -60°$ when the GeTe in TAM is in amorphous (left) or crystalline (right) phase. The thickness of the TAM is $d = 5\mu m$.

This interesting result can also be understood geometrically. We first assume that light impinges onto the TAM in the absence of GeTe films, in which case, there is no reflection

Optics EXPRESS

for all wavelengths and the propagation direction of light won't change due to $\varepsilon_b = \varepsilon_d$. Then inserting ultrathin GeTe films into the TAM along the propagation direction of light (i.e. $\alpha = \theta_i$), the broadband zero-reflection property won't be destroyed. Next, considering the principle of reciprocity by flipping the incident angle from θ_i to $-\theta_i$, the reflection remains as zero when $\theta_i = -\alpha$. Nevertheless, the light entering the TAM will "see" the GeTe films and be affected by them, but with no reflection. In this way, we can tune the light transmission/absorption through changing the phase states of GeTe without any reflection, thus realizing the broadband perfect transmission-to-absorption switching.

Superior to the configuration of $\varepsilon_b \neq \varepsilon_d$, the value of tilt angle α can be arbitrarily chosen in the configuration of $\varepsilon_b = \varepsilon_d$. This unique feature suggests that through harnessing the local tilt angle of each GeTe film, it is possible to obtain dynamically switchable functionality in gradient TAMs for light with almost arbitrary wavefront.

As an example, we propose a gradient TAM that can realize the perfect switching behavior for light with a cylindrical wavefront. The TAM consists of ultrathin GeTe films in a SiO_2 host, as shown schematically in the upper panel in Fig. 7(a). The tilt angle of GeTe films at different transversal positions is engineered, so that the condition $\theta_i = -\alpha$ is satisfied locally for emitted light from a point source (lower panel). Based on the above analysis, we know that the emitted light from the point source in the lower plane can penetrate into the TAM with no reflection and then be controlled by the embedded GeTe films. The numerical verification is performed through examining the radiation of a vertical electric dipole source (dipole moment 1A·m) above the TAM. Figure 7(b) displays simulated H_x-distributions for $\lambda_0 = 4\mu m$ (left) and $\lambda_0 = 7\mu m$ (right) when GeTe is in amorphous (upper) or crystalline (lower) phase. Here, transition boundary condition is applied to the GeTe films for simplicity. The well-defined dipole radiation patterns without clear interference patterns induced by reflection indicate the near-omnidirectional zero reflection on the TAM. As expected, the emitted light in the lower plane can totally transmit through the TAM with GeTe in amorphous phase, while is almost perfectly absorbed by the TAM with GeTe in crystalline phase, irrespective of the working wavelength.

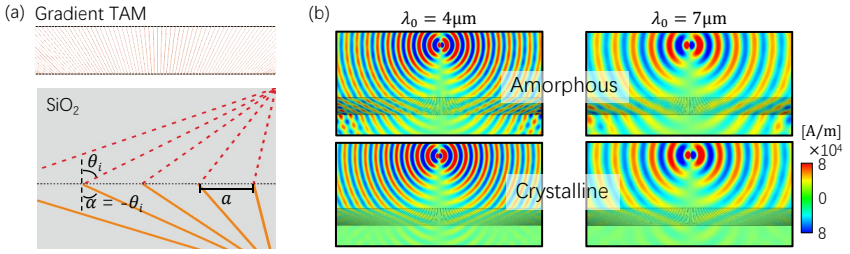

Fig. 7. (a) Upper panel: schematic graph of a gradient TAM consisting of GeTe films with varied tilt angle α. Lower panel: the tilt angle of GeTe films varies with the transversal position, and satisfies the condition $\theta_i = -\alpha$ everywhere for emitted light from a point source. (b) Simulated H_x-distributions when an electric dipole source of $\lambda_0 = 4\mu m$ (left) and $\lambda_0 = 7\mu m$ (right) is placed above the gradient TAM in the SiO_2 background. The upper and lower panels correspond to the TAMs with GeTe in amorphous and crystalline phases, respectively.

5. Conclusion

In summary, we have demonstrated a simple but highly efficient approach to realize broadband perfect transmission-to-absorption switching using TAMs consisting of ultrathin PCM films. Through changing the phase states of the PCM, the functionality of the TAM can be dynamically

Optics EXPRESS

switched from perfect transparency to perfect absorption. Compared with the newly emerging schemes based on resonant meta-structures [29–34], our proposed TAM is non-resonant, and therefore the operating bandwidth can cover a broad spectrum. The underlying physics of the reflectionless transmission/absorption manipulation lies in the anomalous Brewster effect. In addition, we have demonstrated gradient TAMs exhibiting dynamically switchable functionality for incident light with almost arbitrary wavefront. Our proposed TAMs are quite flexible in the material selection of both dielectric hosts and PCMs. Any dielectric material possessing low dissipation loss and low chromatic dispersion can be utilized. Besides the studied GeTe, other PCMs that possess a reversible phase transition under external bias can also be exploited, such as vanadium dioxide (VO_2) [11–13] and germanium antimony telluride ($Ge_2Sb_2Te_5$) [14–17]. Moreover, we find that the switching functionality is quite robust against the variations of geometrical parameters of the TAMs. Our findings offer a simple path towards high-efficiency dynamically controllable functionality with a broad bandwidth.

Funding. Priority Academic Program Development of Jiangsu Higher Education Institutions; National Natural Science Foundation of China (61802272); Hui-Chun Chin and Tsung-Dao Lee Chinese Undergraduate Research Endowment (CURE).

Disclosures. The authors declare no competing financial interest.

Data availability. Data underlying the results presented in this paper are not publicly available at this time but may be obtained from the authors upon reasonable request.

References

1. O. Hess, J. B. Pendry, S. A. Maier, R. F. Oulton, J. M. Hamm, and K. L. Tsakmakidis, "Active nanoplasmonic metamaterials," Nat. Mater. **11**(7), 573–584 (2012).
2. A. E. Minovich, A. E. Miroshnichenko, A. Y. Bykov, T. V. Murzina, D. N. Neshev, and Y. S. Kivshar, "Functional and nonlinear optical metasurfaces," Laser Photonics Rev. **9**(2), 195–213 (2015).
3. S. Liu and T. J. Cui, "Concepts, working principles, and applications of coding and programmable metamaterials," Adv. Opt. Mater. **5**(22), 1700624 (2017).
4. M. Wuttig, H. Bhaskaran, and T. Taubner, "Phase-change materials for non-volatile photonic applications," Nat. Photonics **11**(8), 465–476 (2017).
5. S. Sun, Q. He, J. Hao, S. Xiao, and L. Zhou, "Electromagnetic metasurfaces: physics and applications," Adv. Opt. Photonics **11**(2), 380 (2019).
6. T. Cui, B. Bai, and H. B. Sun, "Tunable metasurfaces based on active materials," Adv. Funct. Mater. **29**(10), 1806692 (2019).
7. A. M. Shaltout, V. M. Shalaev, and M. L. Brongersma, "Spatiotemporal light control with active metasurfaces," Science **364**(6441), eaat3100 (2019).
8. A. Minovich, J. Farnell, D. N. Neshev, I. McKerracher, F. Karouta, J. Tian, D. A. Powell, I. V. Shadrivov, H. Hoe Tan, C. Jagadish, and Y. S. Kivshar, "Liquid crystal based nonlinear fishnet metamaterials," Appl. Phys. Lett. **100**(12), 121113 (2012).
9. D. Shrekenhamer, W. Chen, and W. J. Padilla, "Liquid crystal tunable metamaterial absorber," Phys. Rev. Lett. **110**(17), 177403 (2013).
10. A. Komar, R. Paniagua-Domínguez, A. Miroshnichenko, Y. F. Yu, Y. S. Kivshar, A. I. Kuznetsov, and D. Neshev, "Dynamic beam switching by liquid crystal tunable dielectric metasurfaces," ACS Photonics **5**(5), 1742–1748 (2018).
11. M. A. Kats, D. Sharma, J. Lin, P. Genevet, R. Blanchard, Z. Yang, M. M. Qazilbash, D. N. Basov, S. Ramanathan, and F. Capasso, "Ultra-thin perfect absorber employing a tunable phase change material," Appl. Phys. Lett. **101**(22), 221101 (2012).
12. Z. Jia, F. Shu, Y. Gao, F. Cheng, R. Peng, R. Fan, Y. Liu, and M. Wang, "Dynamically switching the polarization state of light based on the phase transition of vanadium dioxide," Phys. Rev. Appl. **9**(3), 034009 (2018).
13. T. G. Folland, A. Fali, S. T. White, J. R. Matson, S. Liu, N. A. Aghamiri, J. H. Edgar, R. F. Haglund, Y. Abate, and J. D. Caldwell, "Reconfigurable infrared hyperbolic metasurfaces using phase change materials," Nat. Commun. **9**(1), 4371 (2018).
14. C. H. Chu, M. L. Tseng, J. Chen, P. C. Wu, Y. Chen, H. Wang, T. Chen, W. T. Hsieh, H. J. Wu, G. Sun, and D. P. Tsai, "Active dielectric metasurface based on phase-change medium," Laser Photonics Rev. **10**(6), 986–994 (2016).
15. A. Karvounis, B. Gholipour, K. F. MacDonald, and N. I. Zheludev, "All-dielectric phase-change reconfigurable metasurface," Appl. Phys. Lett. **109**(5), 051103 (2016).
16. W. Dong, Y. Qiu, X. Zhou, A. Banas, K. Banas, M. B. H. Breese, T. Cao, and R. E. Simpson, "Tunable mid-infrared phase-change metasurface," Adv. Opt. Mater. **6**(14), 1701346 (2018).
17. C. Ruiz De Galarreta, I. Sinev, A. M. Alexeev, P. Trofimov, K. Ladutenko, S. Garcia-Cuevas Carrillo, E. Gemo, A. Baldycheva, J. Bertolotti, and C. David Wright, "Reconfigurable multilevel control of hybrid all-dielectric phase-change metasurfaces," Optica **7**(5), 476 (2020).

Optics EXPRESS

18. E. Maguid, I. Yulevich, M. Yannai, V. Kleiner, M. L. Brongersma, and E. Hasman, "Multifunctional interleaved geometric-phase dielectric metasurfaces," Light: Sci. Appl. **6**(8), e17027 (2017).
19. Z. Deng, Y. Cao, X. Li, and G. P. Wang, "Multifunctional metasurface: from extraordinary optical transmission to extraordinary optical diffraction in a single structure," Photonics Res. **6**(5), 443 (2018).
20. H. Hajian, A. Ghobadi, A. E. Serebryannikov, B. Butun, G. A. E. Vandenbosch, and E. Ozbay, "VO2-hBN-graphene-based bi-functional metamaterial for mid-infrared bi-tunable asymmetric transmission and nearly perfect resonant absorption," J. Opt. Soc. Am. B **36**(6), 1607 (2019).
21. J. Luan, S. Yang, D. Liu, and M. Zhang, "Polarization and direction-controlled asymmetric multifunctional metadevice for focusing, vortex and Bessel beam generation," Opt. Express **28**(3), 3732 (2020).
22. M. Aalizadeh, A. E. Serebryannikov, E. Ozbay, and G. A. E. Vandenbosch, "A simple Mie-resonator based meta-array with diverse deflection scenarios enabling multifunctional operation at near-infrared," Nanophotonics **9**(15), 4589–4600 (2020).
23. J. Luo, Y. Yang, Z. Yao, W. Lu, B. Hou, Z. H. Hang, C. T. Chan, and Y. Lai, "Ultratransparent media and transformation optics with shifted spatial dispersions," Phys. Rev. Lett. **117**(22), 223901 (2016).
24. Z. Yao, J. Luo, and Y. Lai, "Photonic crystals with broadband, wide-angle, and polarization-insensitive transparency," Opt. Lett. **41**(21), 5106–5109 (2016).
25. C. M. Watts, X. Liu, and W. J. Padilla, "Metamaterial electromagnetic wave absorbers," Adv. Mater. **24**(23), OP98–OP120 (2012).
26. M. A. Kats and F. Capasso, "Optical absorbers based on strong interference in ultra-thin films," Laser Photonics Rev. **10**(5), 735–749 (2016).
27. L. Feng, P. Huo, Y. Liang, and T. Xu, "Photonic metamaterial absorbers: Morphology engineering and interdisciplinary applications," Adv. Mater. **2019**, 1903787 (2019).
28. T. Zhumabek and C. Valagiannopoulos, "Light trapping by arbitrarily thin cavities," Phys. Rev. Res. **2**(4), 043349 (2020).
29. Y. Li, J. Lin, H. Guo, W. Sun, S. Xiao, and L. Zhou, "A tunable metasurface with switchable functionalities: From perfect transparency to perfect absorption," Adv. Opt. Mater. **8**(6), 1901548 (2020).
30. A. de Lustrac, B. Ratni, G. Piau, Y. Duval, and S. N. Burokur, "Tri-state metasurface-based electromagnetic screen with switchable reflection, transmission, and absorption functionalities," ACS Appl. Electron. Mater. **3**(3), 1184–1190 (2021).
31. H. L. Wang, H. F. Ma, M. Chen, S. Sun, and T. J. Cui, "A reconfigurable multifunctional metasurface for full-space control of electromagnetic waves," Adv. Funct. Mater. **31**(25), 2100275 (2021).
32. R. Phon, S. Ghosh, and S. Lim, "Active frequency selective surface to switch between absorption and transmission band with additional frequency tuning capability," IEEE Trans. Antennas Propag. **67**(9), 6059–6067 (2019).
33. V. Erçağlar, H. Hajian, and E. Özbay, "VO2-graphene-integrated hBN-based metasurface for bi-tunable phonon-induced transparency and nearly perfect resonant absorption," J. Phys. D: Appl. Phys. **54**(24), 245101 (2021).
34. Y. Ren, T. Zhou, C. Jiang, and B. Tang, "Thermally switching between perfect absorber and asymmetric transmission in vanadium dioxide-assisted metamaterials," Opt. Express **29**(5), 7666 (2021).
35. K. Liu, C. R. Ye, S. Khan, and V. J. Sorger, "Review and perspective on ultrafast wavelength-size electro-optic modulators," Laser Photonics Rev. **9**(2), 172–194 (2015).
36. Y. Qu, Q. Li, K. Du, L. Cai, J. Lu, and M. Qiu, "Dynamic thermal emission control based on ultrathin plasmonic metamaterials including phase-changing material GST," Laser Photonics Rev. **11**(5), 1700091 (2017).
37. J. Xu, J. Mandal, and A. P. Raman, "Broadband directional control of thermal emission," Science **372**(6540), 393–397 (2021).
38. H. F. Hamann, M. O'Boyle, Y. C. Martin, M. Rooks, and H. K. Wickramasinghe, "Ultra-high-density phase-change storage and memory," Nat. Mater. **5**(5), 383–387 (2006).
39. D. W. Ferrara, J. Nag, E. R. MacQuarrie, A. B. Kaye, and R. F. Haglund, "Plasmonic probe of the semiconductor to metal phase transition in vanadium dioxide," Nano Lett. **13**(9), 4169–4175 (2013).
40. N. Yamada, E. Ohno, K. Nishiuchi, N. Akahira, and M. Takao, "Rapid-phase transitions of GeTe-Sb2Te3 pseudobinary amorphous thin films for an optical disk memory," J. Appl. Phys. **69**(5), 2849–2856 (1991).
41. C. M. Chang, C. H. Chu, M. L. Tseng, H. Chiang, M. Mansuripur, and D. P. Tsai, "Local electrical characterization of laser-recorded phase-change marks on amorphous Ge2Sb2Te5 thin films," Opt. Express **19**(10), 9492 (2011).
42. D. Loke, T. H. Lee, W. J. Wang, L. P. Shi, R. Zhao, Y. C. Yeo, T. C. Chong, and S. R. Elliott, "Breaking the speed limits of phase-change memory," Science **336**(6088), 1566–1569 (2012).
43. J. Luo, H. Chu, R. Peng, M. Wang, J. Li, and Y. Lai, "Ultra-broadband reflectionless Brewster absorber protected by reciprocity," Light: Sci. Appl. **10**(1), 89 (2021).
44. H. Fan, J. Li, Y. Lai, and J. Luo, "Optical Brewster metasurfaces exhibiting ultrabroadband reflectionless absorption and extreme angular asymmetry," Phys. Rev. Appl. **16**(4), 044064 (2021).
45. M. Chen, K. A. Rubin, and R. W. Barton, "Compound materials for reversible, phase-change optical data storage," Appl. Phys. Lett. **49**(9), 502–504 (1986).
46. M. Jafari, L. J. Guo, and M. Rais Zadeh, "A Reconfigurable Color Reflector by Selective Phase Change of GeTe in a Multilayer Structure," Adv. Opt. Mater. **7**(5), 1801214 (2019).
47. K. Shportko, S. Kremers, M. Woda, D. Lencer, J. Robertson, and M. Wuttig, "Resonant bonding in crystalline phase-change materials," Nat. Mater. **7**(8), 653–658 (2008).

Optics EXPRESS

48. V. A. Markel, "Introduction to the Maxwell Garnett approximation: tutorial," J. Opt. Soc. Am. A **33**(7), 1244 (2016).
49. T. Dong, J. Luo, H. Chu, X. Xiong, R. Peng, M. Wang, and Y. Lai, "Breakdown of Maxwell Garnett theory due to evanescent fields at deep-subwavelength scale," Photonics Res. **9**(5), 848 (2021).
50. D. Brewster, "On the laws which regulate the polarisation of light by reflexion from transparent bodies," Phil. Trans. R. Soc. **105**, 125–159 (1815).
51. J. B. Pendry, A. J. Holden, D. J. Robbins, and W. J. Stewart, "Low frequency plasmons in thin-wire structures," J. Phys.: Condens. Matter **10**(22), 4785–4809 (1998).
52. R. J. Potton, "Reciprocity in optics," Rep. Prog. Phys. **67**(5), 717–754 (2004).
53. https://refractiveindex.info/?shelf=main&book=SiO2&page=Kischkat.
54. D. W. Berreman, "Optics in stratified and anisotropic media: 4×4-matrix formulation," J. Opt. Soc. Am. **62**(4), 502–510 (1972).